Assessment of Stability Differences in the Protein G B1 and B2 Domains From Hydrogen−Deuterium Exchange: Comparison with Calorimetric Data†

John Orban,* Patrick Alexander, Philip Bryan, and Devesh Khare

Center for Advanced Research in Biotechnology, University of Maryland Biotechnology Institute, 9600 Gudelsky Drive, Rockville, Maryland 20850

Received June 6, 1995; Revised Manuscript Received August 17, 1995®

ABSTRACT: Hydrogen−deuterium (H−D) exchange experiments have been used to measure exchange rates for almost all of the main-chain amide protons (NHs) in the B1 and B2 IgG-binding domains of protein G. For H-bonded NHs, exchange rates were also measured as a function of temperature from 25 to 65 °C for B1 and from 25 to 60 °C for B2. A number of NHs exchange by a mechanism consistent with global unfolding. For these residues, the free energy required for transient opening of a H-bonded NH (ΔG_{op}) from H−D exchange approximates the extrapolated free energy of thermal unfolding (ΔG_u) from calorimetry in B1 and B2. The difference in exchange rates between B1 and B2 for these residues reflects the 1 kcal mol^{-1} difference in stability from calorimetry. The more stable B1 domain appears to have a slightly larger core of residues which exchange by global unfolding than B2. The ΔG_{op} values for slow exchange H-bonded NHs and calorimetric ΔG_u provide highly complementary information on the ΔG versus temperature stability profiles of B1 and B2. Furthermore, NH exchange rates provide a very sensitive measure of local stability differences between B1 and B2. In both domains, the β2-strand is the least stable of the β−sheet although it is more stable in B1 than B2. The largest local stability differences occur at residues Y3 and T18 which exchange 40-fold and 100-fold slower in B1, respectively. These residues form a H-bond donor−acceptor pair at one end of the β1−β2 hairpin region. Local stability differences are also evident near the β1−β2 turn. These stability differences are, at least in part, due to subtle differences in hydrophobic packing effects. They are not obvious from inspection of the B1 and B2 structures but are manifested as readily measurable changes in NH exchange rates for individual residues. Knowledge of these local stability differences in the β1−β2 region provides potential approaches for designing new stability mutants in protein G. Most non-H-bonded NHs have exchange rates that are <15 times slower than their intrinsic rates. In marked contrast, the NHs of K10, T11, and L12 in the β1−β2 turn and V21 have exchange rates which are five to ≥24 times *faster* than their intrinsic rates, probably due to local electrostatic effects. For some slow exchanging NHs, particularly in the β3−β4 hairpin region, the ΔG_{op} value is greater than ΔG_u by up to 1 kcal mol^{-1}, suggesting that some residual structure may exist in the "unfolded state".

Protein G is a multidomain cell wall protein that occurs in streptococcus and contains two to three immunoglobulin G (IgG)-binding domains, designated here as B1 and B2. These small 56 amino acid domains differ by six amino acid substitutions and bind the constant Fc region of IgG tightly with $K_a \approx 10^8$ M^{-1} (Myhre & Kronvall, 1977; Reis et al., 1984; Fahnestock et al., 1986). The IgG-binding domains of protein G are similar in size to those of staphylococcal protein A (Åkerstrom & Bjorck, 1986), and protein G and protein A compete for binding at the C_{H2}−C_{H3} interface of IgG (Wright et al., 1977; Stone et al., 1989). The two proteins have no sequence or structural homology, however. Protein A is a three−helix bundle (Gouda et al., 1992), whereas the IgG-binding domain of protein G consists of a four-stranded β-sheet packed against a helix (Gronenborn et al., 1991; Achari et al., 1992; Lian et al., 1991, 1992; Orban et al., 1992; Gallagher et al., 1994).

From differential scanning calorimetry, the B1 and B2 domains exhibit reversible two-state unfolding behavior over a wide pH range with denaturation temperatures of 87.5 and 79.4 °C, respectively, at pH 5.4 (Alexander et al., 1992). Since the heat capacity difference, ΔC_p, is known for B1 and B2, ΔG_u can be calculated for temperatures outside the calorimetrically measurable range using the Gibbs−Helmholtz equation

$$\Delta G_u = \Delta H_0 - T\Delta S_0 + \Delta C_p[T - T_0 - T\ln(T/T_0)] \quad (1)$$

where ΔH_0 and ΔS_0 are the enthalpy and entropy of unfolding at a reference temperature T_0 and ΔG_u is the free energy of unfolding at a temperature T (Brandts, 1964; Pace & Tanford, 1968; Privalov & Khechinashvili, 1974; Privalov, 1979; Becktel & Schellman, 1987). Using eq 1, the extrapolated free energy of thermal unfolding, ΔG_u, is 6.6 kcal mol^{-1} for B1 and 5.6 kcal mol^{-1} for B2, at 25 °C. The relatively large change in denaturation temperature occurs because the stability profile (ΔG_u versus temperature) is flat and shallow due to the small ΔS and ΔC_p for unfolding. In addition to thermodynamic analysis by calorimetric methods (Alexander et al., 1992), kinetic analysis of the folding and unfolding of both domains has been carried out using stopped-flow mixing techniques (Alexander et al., 1992).

† Supported by NSF Grant MCB-92-19309.
* Author to whom correspondence should be addressed.
® Abstract published in *Advance ACS Abstracts,* November 1, 1995.

0006-2960/95/0434-15291$09.00/0

Stability parameters can also be obtained from measurement of hydrogen−deuterium (H−D) exchange rates of labile main-chain amide (NH) protons (Bai et al., 1994). Amide exchange rates can be analyzed in terms of the structural unfolding model (Hvidt & Nielsen, 1966), in which the exchange mechanism can be described by the reaction path shown in eq 2.

$$\mathrm{F(H)} \underset{k_f}{\overset{k_u}{\rightleftharpoons}} \mathrm{U(H)} \xrightarrow[\mathrm{D_2O}]{k_c} \mathrm{U(D)} \underset{k_u}{\overset{k_f}{\rightleftharpoons}} \mathrm{F(D)} \qquad (2)$$

In this scheme, k_u, k_f, and k_c are the unfolding, folding, and intrinsic exchange rates, respectively, F is the native or folded state, and U represents open or unfolded states. Under stabilizing conditions, $k_f \gg k_u$, $k_f \gg k_c$ (EX_2 limit), and the measured exchange rate, k_{ex}, is given by

$$k_{ex} = k_u k_c / k_f = K_{op} k_c \qquad (3)$$

The free energy required for transient opening is then

$$\Delta G_{op} = -RT \ln K_{op} = -RT \ln(k_{ex}/k_c) \qquad (4)$$

where K_{op} is the equilibrium constant for transient opening and ΔG_{op} is the free energy difference between folded and locally or globally unfolded states.

Here, we report exchange rates for nearly all of the main-chain NHs in B1 and B2 at 25 °C. A number of NHs exchange by a mechanism consistent with global unfolding. For these residues, the ΔG_{op} value approximates the extrapolated ΔG_u in B1 and B2. The difference in exchange rates between B1 and B2 reflects the 1 kcal mol^{-1} difference in stability from calorimetry. For H-bonded NHs, exchange rates were also measured as a function of temperature. The ΔG_{op} values for slow exchange H-bonded NHs and ΔG_u from calorimetry provide highly complementary information on the stability profiles of B1 and B2. Furthermore, in contrast to the macroscopic stability parameter (ΔG_u) from calorimetry, NH exchange rates provide a very sensitive measure of local stability differences between B1 and B2. Knowledge of these local stability differences provides potential avenues for engineering new stability mutants for protein G. For non-H-bonded NHs, exchange rates are compared with their calculated intrinsic rates. Finally, some residues have ΔG_{op} values up to 1 kcal mol^{-1} greater than the extrapolated ΔG_u at 25 °C, and the implications of these results with regard to the unfolded state are discussed.

MATERIALS AND METHODS

Sample Preparation and NMR Spectroscopy. The protein G B1 and B2 domains were cloned, expressed, and purified as described in Alexander et al. (1992). Uniformly ^{15}N-labeled samples (≥95%) were prepared by expression in M9 minimal media with $^{15}NH_4Cl$ as the sole nitrogen source. NMR samples for assignment of resonances were prepared by dissolving lyophilized protein in 0.4 mL of 100 mM NaOAc-d_3 buffer, pH 5.4, containing 10% D_2O. Low-pH experiments were carried out by adjusting samples to pH 3.1 using small aliquots of 2 M HCl solutions. Sample concentrations for B1 and B2 were 5 mM. NMR spectra were recorded on a Bruker AMX-500 and processed on Silicon Graphics workstations using FTNMR or FELIX (Biosym, San Diego, CA). ^{1}H−^{15}N heteronuclear single-quantum coherence (HSQC; Bodenhausen & Ruben, 1980; Bax et al., 1990; Norwood et al., 1990) spectra were acquired in time-proportional phase incrementation (TPPI; Marion & Wuthrich, 1983) mode with no phase cycling (Marion et al., 1989) using 256 t_1 increments and spectral widths of 5000 and 1670 Hz in the ^{1}H and ^{15}N dimensions, respectively. ^{15}N-decoupling during t_2 was achieved using a GARP sequence (Shaka et al., 1985). The $1/(4J_{NH})$ delay was set to 2.3 ms, and the relaxation delay was 1.0 s. ^{1}H−^{15}N HMQC−COSY and HMQC−NOESY spectra (Gronenborn et al., 1989) were acquired using 800 t_1 increments of 2 K data points with 32 or 64 transients per increment and spectral widths of 6024 Hz and 1670 Hz in the ^{1}H and ^{15}N dimensions, respectively. The $1/(2J_{NH})$ delay was set to 4 ms. A relaxation delay of 2.0 s was used, and the mixing time was 200 ms in the HMQC−NOESY experiment. The water signal was suppressed using solvent presaturation. Chemical shifts were referenced to the carrier in F1 (118.2 ppm) and F2 (4.77 ppm) at 25 °C.

Determination of Amide Proton Exchange Rates. The lyophilized protein was dissolved in 99.99% D_2O, the pD was adjusted to 5.7 (meter reading), and the HSQC spectra were recorded at a series of time intervals at 25 °C. No solvent suppression was employed in D_2O spectra, and the total measurement time per spectrum was ~5.7 min using 256 t_1 increments and a relaxation delay of 1.0 s. The decays in integrated peak volumes of individual NHs were fitted to first-order exponential curves of the form $A_t = A_0 \exp(-k_{ex}t)$, where A_t is the peak volume at time t and k_{ex} is the first-order rate constant. Fifteen to twenty time points were obtained for each domain, with time points ranging from 15 min to 500 h for B1 and from 15 min to 140 h for B2. Samples were not removed from the magnet during the time course. Volumes were normalized to the upfield-shifted nonexchangeable γ-methyl resonance of V54 obtained from one-dimensional proton spectra. The integral of this signal did not change during the course of the experiments. HSQC spectra were also recorded with a relaxation delay of 2.0 s during the time course. Exchange rate measurements from these spectra were within ±10% of those obtained from the 1.0 s data for most residues and within ±20% for all residues. The latter error limit corresponds to a ±20% error in $\Delta\Delta G_{op}$ values for residues with the same intrinsic rate in B1 and B2 (from eq 4).

Exchange rates obtained at elevated temperatures were either from HSQC spectra recorded with 256 or 80 t_1 increments (40 and 50 °C data) or from one-dimensional ^{1}H−^{15}N heteronuclear multiple-quantum coherence (HMQC) spectra (55−65 °C data). One-dimensional HMQC spectra (Bax et al., 1983) were recorded with 2 or 4 transients per spectrum and set up in automation mode for rapid recording of spectra in series. The $1/(2J_{NH})$ delay was set to 4.5 ms, and the relaxation delay was 1.0 s. Temperatures were regulated by the variable temperature unit on the spectrometer and calibrated against a standard solution of ethylene glycol in DMSO-d_6.

Rates for fast exchanging NHs at pD 3.1 ($k > 1$ h^{-1}) were obtained from HSQC spectra recorded with 80 t_1 increments and a relaxation delay of 1.0 s, making the total measurement time ~1.8 min per spectrum. The use of automation programs permitted the collection of 10 time points in less than 20 min. In this case, the pD was checked after the collection of the time course. The dead time between addition of D_2O to the lyophilized protein and the start

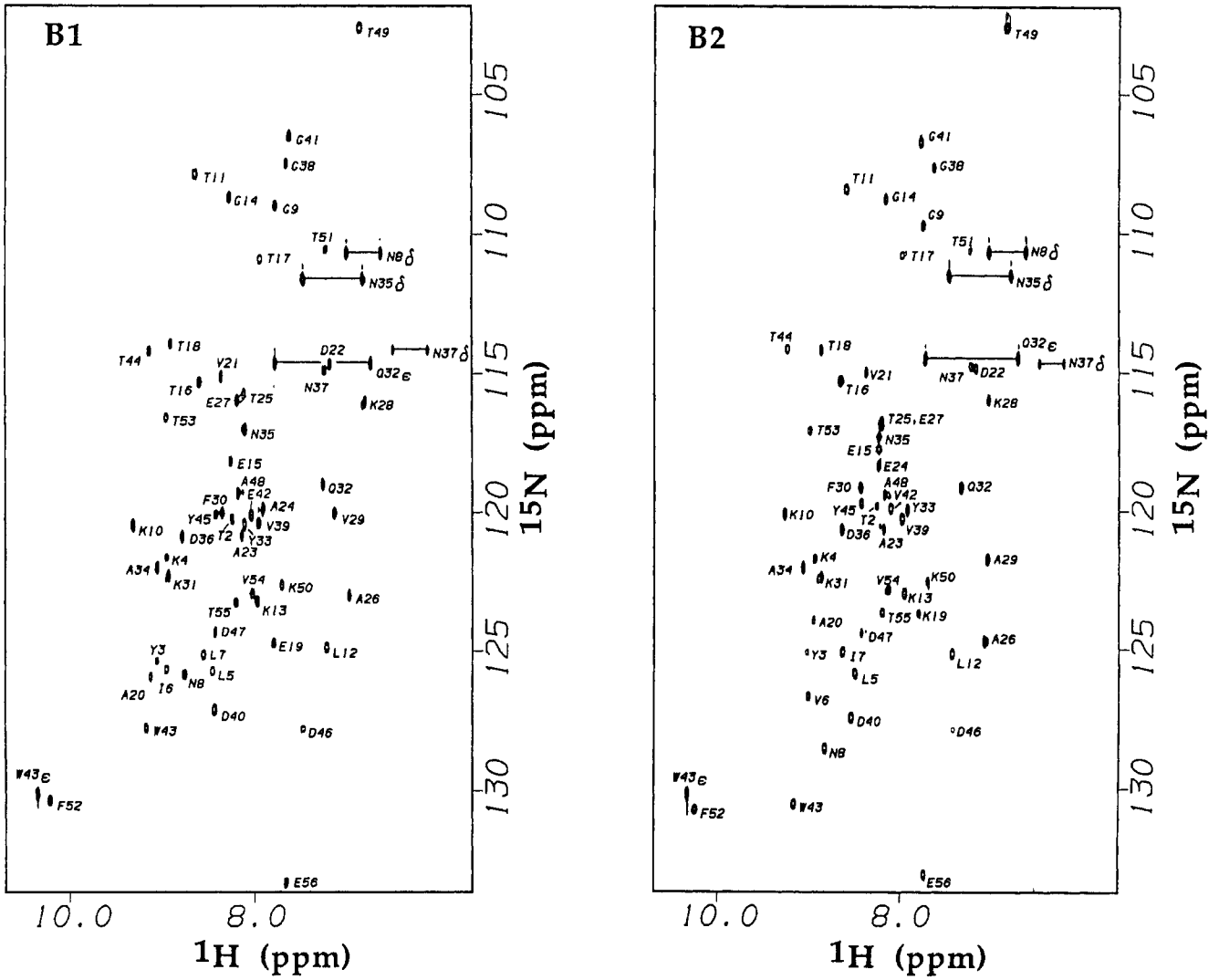

FIGURE 1: $^{1}H-^{15}N$ HSQC spectra of the B1 and B2 domains of protein G at pH 5.4, 25 °C.

of data acquisition was 2.7 min.

Random coil intrinsic exchange rates were corrected for the appropriate pH and temperature using the method detailed by Bai et al. (1993).

RESULTS

Chemical shift assignments were obtained in a straightforward manner. $^{1}H-^{15}N$ HMQC–COSY spectra provided backbone amide ^{15}N to NH and αCH correlations within an amino acid residue. Sequence-specific assignments of ^{15}N resonances were then made by comparing these correlations with NH and αCH chemical shifts obtained from homonuclear experiments (Orban et al., 1992). As an additional check, the sequential main-chain assignments were confirmed from analysis of $^{1}H-^{15}N$ HMQC–NOESY spectra. HMQC–COSY and HMQC–NOESY spectra (not shown) were recorded at pH 5.4 and 3.1. Assigned HSQC spectra of B1 and B2 are shown in Figure 1, and chemical shift difference plots are shown in Figure 2. The ^{1}H and ^{15}N chemical shifts for main-chain NHs in B1 and B2 are summarized in Table 1 of the supporting information.

Exchange rates were measured for 32 slowly exchanging H-bonded NHs in B1 and B2 at pD 5.7, 25 °C. Rates for 21 fast exchanging NHs, most of which are non-H-bonded, were also measured directly from H–D exchange experiments at pD 3.1, 25 °C, using $^{1}H-^{15}N$ HSQC spectra acquired with 80 t_1 increments. These rates are summarized in Table 1. Representative decay curves are shown in Figure 3. Exchange rates could not be obtained for A48 in B1 or B2 due to overlap at pD 3.1. A ΔG_{op} value was calculated for each residue using eq 4, and these values were compared with the extrapolated ΔG_u from calorimetry (Figure 4). In B1, residues with slow exchanging NHs in the β1-, β2-, β3-, and β4-strands as well as the helix have ΔG_{op} values that approximate the extrapolated ΔG_u. In B2, ΔG_{op} values for slow exchangers are more clustered than in B1. In both domains, the β2-strand is the least stable of the β-sheet although it is more stable in B1 than B2. For some slow exchanging NHs, particulary in the β3–β4 hairpin region (residues 42–56), the ΔG_{op} value is greater than ΔG_u by up to 1 kcal mol^{-1}. Thus, the β3–β4 hairpin region is more stable than the β1–β2 hairpin region (residues 1–20). In addition, slow exchange NHs in the N-terminal part of the helix have higher ΔG_{op} values than in the C-terminal part of the helix. This is more evident in the B1 domain since ΔG_{op} values for slow exchange NHs are more spread out than in B2.

Figure 5 shows a plot of $\Delta\Delta G_{op}$(B1–B2) versus residue number. For a number of residues with $\Delta G_{op} \approx \Delta G_u$, the $\Delta\Delta G_{op}$ is consistent with the calorimetric difference in global

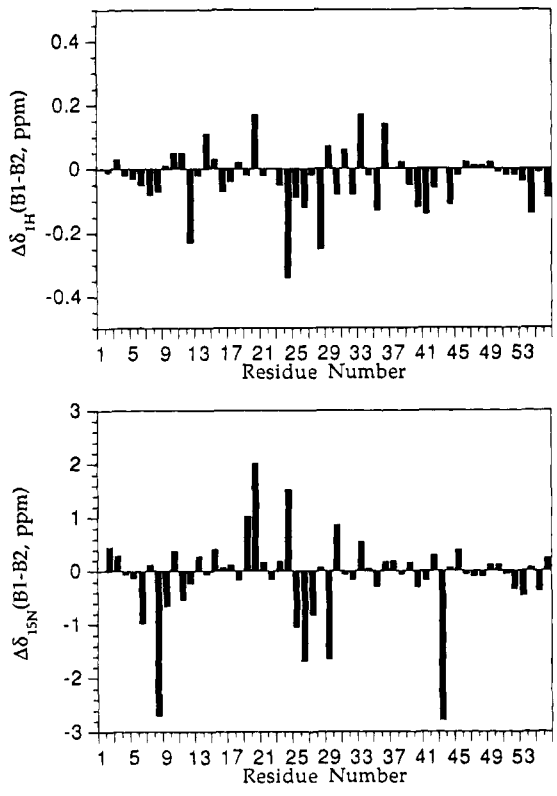

FIGURE 2: ^1H and ^{15}N chemical shift difference (B1 − B2) plots for main-chain amide protons (top) and nitrogens (bottom) at pH 5.4, 25 °C.

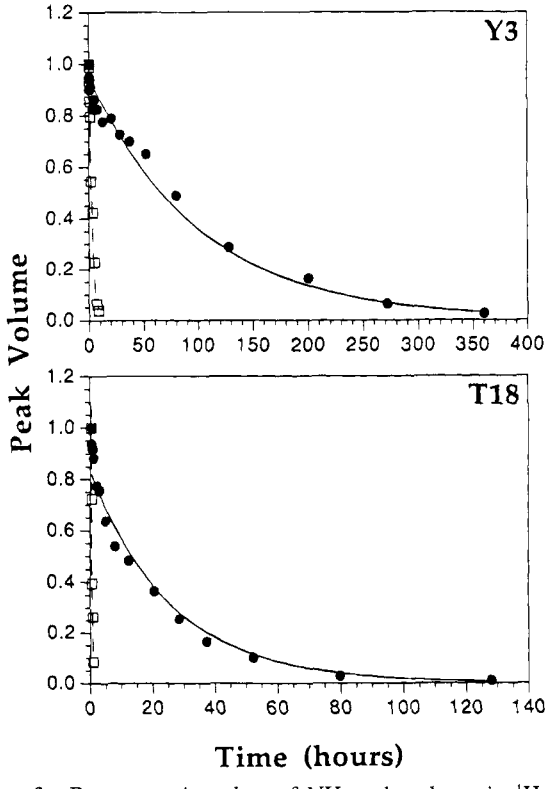

FIGURE 3: Representative plots of NH peak volume in $^1H-^{15}N$ HSQC spectra versus exchange time in B1 (filled circles) and B2 (open squares) at 25 °C.

stability, which is ca. 1 kcal mol^{-1} (Alexander et al., 1992). The NHs of these residues exchange by a mechanism consistent with global unfolding. The $\Delta\Delta G_{op}$ values were mapped onto the three-dimensional X-ray structure of B1

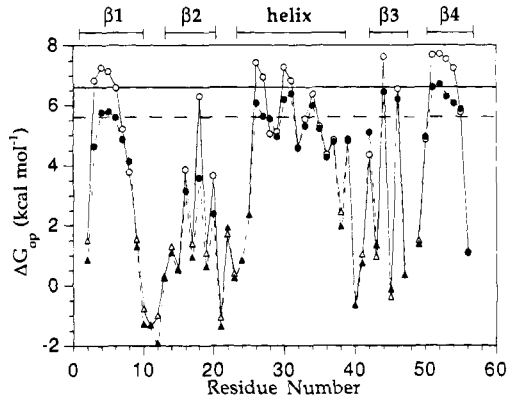

FIGURE 4: Plot of ΔG_{op} versus residue number for B1 (open circles/triangles) and B2 (filled circles/triangles) at 25 °C. Slow exchanging NHs were measured at pD 5.7 (circles), and fast exchanging NHs were measured at pD 3.1 (triangles). Note that the ΔG_{op} values are upper limits for T11, D40, and D47 in B1 and T2, K10, T11, L12, D40, and D47 in B2. For comparison with the pD 5.7 ΔG_{op} values, the horizontal lines represent the extrapolated ΔG_u for B1 (solid line) and B2 (broken line) from calorimetry at pH 5.4, 25 °C.

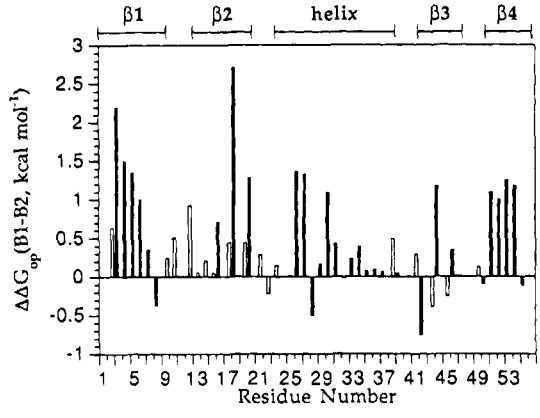

FIGURE 5: Plot of $\Delta\Delta G_{op}$(B1−B2) versus residue number. Values were determined at pD 5.7 (filled bars) and pD 3.1 (open bars). Note that $\Delta\Delta G_{op}$ values are lower limits for residues T2, K10, T11, L12, D40, and D47.

(Gallagher et al., 1994), and the results are summarized in Figure 6. In addition, the temperature dependence of slow exchange NHs was monitored and the ΔG_{op} values were compared with ΔG_u extrapolated from calorimetric data using the Gibbs−Helmholtz relationship (Alexander et al., 1992). Figure 7 and Table 1 summarize the temperature dependent results.

Local stability differences were detected in the $\beta1-\beta2$ hairpin region where relatively large $\Delta\Delta G_{op}$ values (>2 kcal mol^{-1}) were observed for Y3 and T18. Stability differences were also observed in the $\beta1-\beta2$ turn, particularly for L12 where $\Delta\Delta G_{op} \geq 0.9$ kcal mol^{-1}.

Most non-H-bonded NHs have fast exchange rates (≥ 1 h^{-1} at pD 3.1, 25 °C) which are <15 times slower than their intrinsic rates. However, several residues in the $\beta1-\beta2$ turn (K10, T11, L12) and V21 have NH exchange rates which are five to ≥24 times *faster* than their intrinsic rates (Table 1), resulting in negative ΔG_{op} values (Figure 4).

DISCUSSION

Local vs Global Unfolding. The mechanism for exchange of H-bonded main-chain NHs in proteins has been reviewed extensively [e.g., Woodward et al. (1982), Wagner (1983),

Table 1: Main-Chain Amide Proton Exchange Rates (h^{-1}) for the B1 and B2 Domains of Protein G from 25 to 60 °C[a]

	B1						B2				
residue	k_{25}	k_{40}	k_{50}	k_{55}	k_{60}	k_{65}	k_{25}	k_{40}	k_{50}	k_{55}	k_{60}
M1											
T2[b]	22(280)						≥65(280)				
Y3	0.0098	0.68	15				0.40	7.5			
K4	0.0057	0.31	6.0[d]	32[d]			0.071	3.0	31	93	170
L5	0.0024	0.20	6.6	19	65	150	0.023	1.5	22	75	160
I6V[c]	0.0020	0.066	1.5	14			0.012	0.56	18		
L7I[c]	0.027	0.45	4.5	22	65	160	0.043	1.2	21	69	110
N8	3.8	17					2.0	26			
G9[b]	1.8(24)						2.7(24)				
K10[b]	32(8.8)						≥65(8.8)				
T11[b]	≥65(7.0)						≥65(7.0)				
L12[b]	14(2.7)						≥65(2.7)				
K13[b]	2.2(3.7)						2.4(3.7)				
G14[b]	1.7(15)						2.4(15)				
E15[b]	6.2(16)						6.7(16)				
T16	1.0	7.1	40		150		3.4				
T17[b]	0.80(8.4)						1.7(8.4)				
T18	0.038	1.5	12	40			3.7				
E19K[b,c]	2.7(17)						3.0(9.0)				
A20	1.7	11	21				28				
V21[b]	8.6(1.4)						14(1.4)				
D22[b]	1.2(22)						0.83(22)				
A23[b]	13(25)						16(25)				
A24E[b,c]							2.6(11)				
T25[b]	0.1(5.4)						0.24(13)				
A26	0.0065	0.42	3.6	25	85	160	0.065	3.7	33	110	140
E27	0.0029	0.12	3.2	15			0.027	1.2	39		
K28	0.15	1.2	6.4	22	69	110	0.064	1.5	39	90[g]	150[g]
V29A[c]	0.053	0.52	2.4	9.8	37	88	0.35	3.5	47	90[g]	150[g]
F30	0.0022	0.13	2.0	19	56	120	0.019	0.95	24	86	170
K31	0.012	0.54	6.8[d]	25[d]			0.025	1.3	33	99	110
Q32	0.78	5.0	17		120	150	0.76	6.9	45	140	150
Y33	0.086	2.0	7.9[e]	26[e]			0.13	2.9	27	89	120
A34	0.028	0.59	14	23			0.054	2.7	28	94	160
N35	0.47	3.6	18		100[f]	150[f]	0.54	6.3	46	100	130
D36	0.77	8.4	43		100	210	0.90	12	63	85[h]	110[h]
N37	0.67	6.0	30				0.74	5.3	38	140	170
G38[b]	0.38(24)						0.87(24)				
V39	0.094	1.8	11	22	48	88	0.10	1.6	16	53	110
D40[b]	≥65(22)						≥65(22)				
G41[b]	8.0(46)						13(46)				
E42V[c]	0.35	0.84	11[e]	30[e]		140	0.063	0.92	26		
W43[b]	1.2(6.1)						0.2(2.0)				
T44	0.0020	0.11	2.3	17	58	110	0.014	0.81	18	62	140
Y45[b]	10(5.4)						6.6(5.4)				
D46	0.010	0.23	4.1	25	59	110	0.019	1.6	27	73	100
D47[b]	≥65(120)						≥65(120)				
A48											
T49[b]	0.43(5.4)						0.53(5.4)				
K50	0.46	4.8	22		99	160	0.40	5.2	25	82	130
T51	0.0030	0.24	4.9	25	79	170	0.019	1.1	41	110	240
F52	0.0024	0.11	4.3	29	83	230	0.013	0.64	30	93	120
T53	0.0034	0.27	5.3	25			0.028	2.2	36		
V54	0.0018	0.16	3.3	22	64	130	0.013	0.95	34		
T55	0.043	0.68	7.7	20	60	120	0.035	1.2	16		
E56	1.5	5.4			50	89	1.5	3.0	15	35	51

[a] Exchange rates were measured at pD 5.7 (meter reading) unless otherwise noted. Blank spaces indicate that rates could not be obtained due either to fast exchange or to peak overlap. [b] Rates were measured at pD 3.1 (meter reading), 25 °C. Intrinsic rates for these residues are in brackets and were calculated assuming protonation of acidic residues. [c] Variant residues (B1 to B2). [d] Cross-peaks due to K4 and K31 are partly overlapped. [e] Cross-peaks due to Y33 and E42 are partly overlapped. [f] N35 resonance is overlapped with half of the T55 doublet in the 1D HMQC spectrum. [g] Rates are due to overlapped K28 and A29 resonances. [h] D36 resonance is overlapped with half of the I7 doublet.

Englander and Kallenbach (1984), and Englander and Mayne (1992)]. It is generally agreed that H-bond breakage must occur for exchange with the solvent to take place. This may occur through a transient unfolding of the relevant residue(s) either by large-amplitude global unfolding of the whole protein or by smaller-amplitude local unfolding mechanisms. Two main criteria for H−D exchange by a global unfolding mechanism can be established. Firstly, ΔG_{op} will approximate ΔG_u, the free energy of unfolding from calorimetry. Secondly, the difference between exchange rates in B1 and B2 [$\Delta\Delta G_{op}$(B1−B2)] for a global unfolder should correspond with the 1 kcal mol^{-1} difference in global stability observed from calorimetry. Therefore, if ΔG_{op} approximates ΔG_u for a given residue and $\Delta\Delta G_{op} \approx 1$ kcal mol^{-1}, then the residue exchanges through a global unfolding mechanism. If exchange rates are unaffected by distant mutational

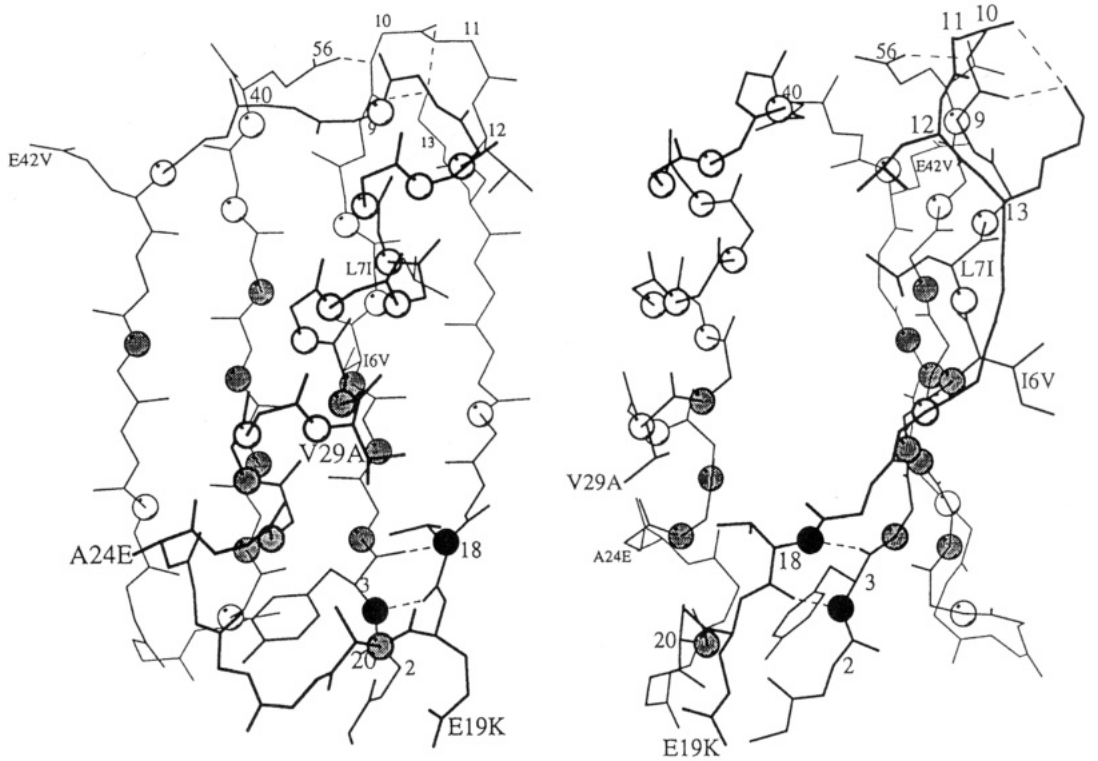

FIGURE 6: Two orthogonal views of the B1 X-ray structure. The $\Delta\Delta G_{op}$(B1−B2) values for individual residues are represented by spheres at the main-chain nitrogen atom positions as follows: $\Delta\Delta G_{op} > 1.5$ kcal mol^{-1} (black spheres), $\Delta\Delta G_{op} \approx 1-1.5$ kcal mol^{-1} (grey spheres), $\Delta\Delta G_{op} < 1$ kcal mol^{-1} (white spheres). Only slow exchange values determined at pD 5.7 are shown here for clarity. Variant residues are labeled with the letter code for both domains (B1 to B2). The figures were generated using MOLSCRIPT (Kraulis, 1991).

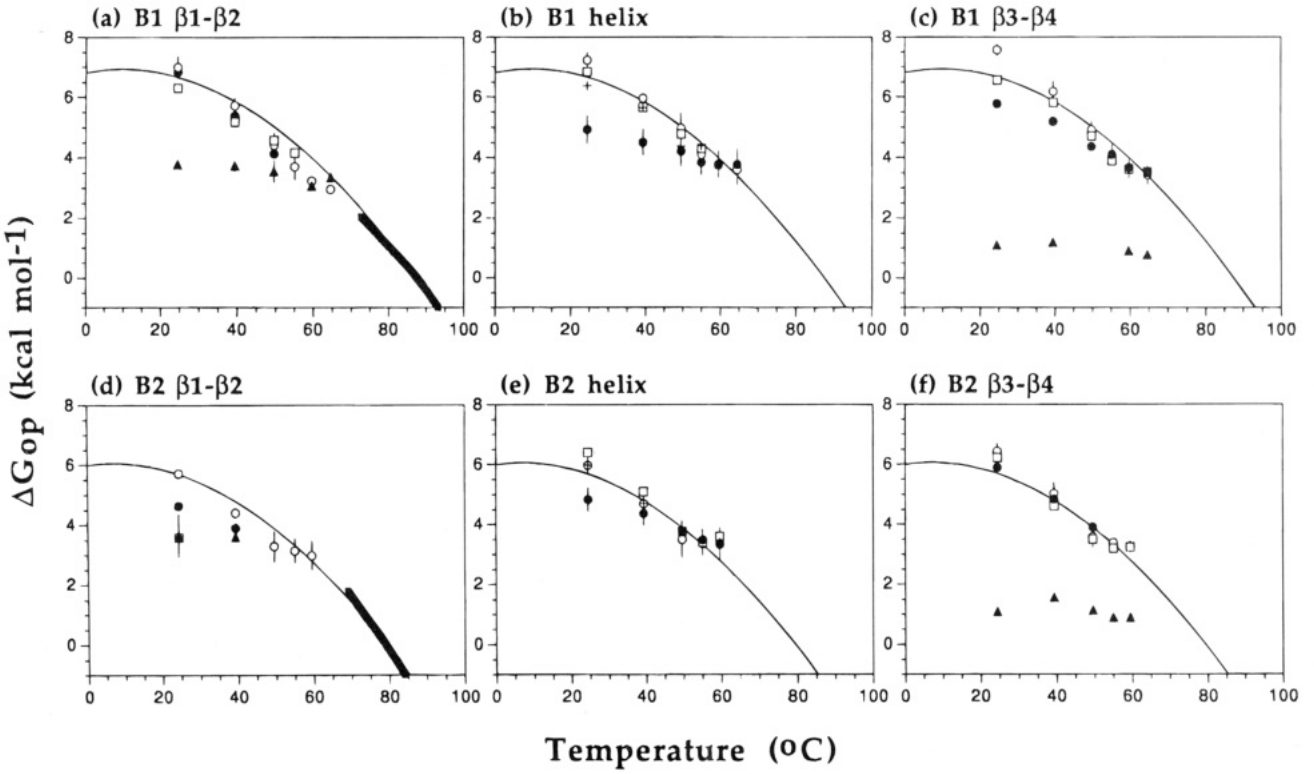

FIGURE 7: Temperature dependence of ΔG_{op} for most of the slow exchanging NHs in B1 and B2. For clarity, separate plots are shown for NHs in the $\beta1-\beta2$, helix, and $\beta3-\beta4$ regions of B1 (a−c) and B2 (d−f). Also, NHs with similar ΔG_{op} values are averaged and plotted with error bars as $\Delta G_{op} \pm$ SD. The calorimetric data points (■) through the thermal transition at pH 5.4 (Alexander et al., 1992) are shown for B1 (a) and B2 (d). The stability profiles in B1 and B2 (solid line) are extrapolated from the calorimetric data using eq 1 in the text. Residues are represented as follows: in a and d, Y3 (●), average of K4, L5, and I6V (○), T18 (□), average of N8, T16 (and A20 in B1) (▲); in b and e, average of A26, E27, and F30 (○), K31 (□), A34 (+), average of Q32, Y33, N35, D36, N37, and V39 (●); in c and f, average of T44, T51, F52, T53, and V54 (○), D46 (□), T55 (●), E56 (▲).

differences in B1 and B2 ($\Delta\Delta G_{op} \approx 0$ kcal mol^{-1}), then the residue exchanges through a local unfolding mechanism.

From inspection of Figures 4 and 5, a number of residues satisfy the above criteria for exchange through a global

unfolding mechanism. These residues are K4, L5, and I6V in the β1-strand; A26, E27, and F30 in the helix; T44 in the β3-strand; and T51, F52, T53, and V54 in the β4-strand. In the X-ray structures (Achari et al., 1992; Gallagher et al., 1994), they are buried from the solvent accessible surface and are located near the center of β-strands and the N-terminal half of the helix (Figure 6). It is interesting to note that the average ΔG_{op} value for T44, T51, F52, T53, and V54 in the $\beta3-\beta4$ hairpin is greater than the extrapolated ΔG_u at 25 °C by 1 kcal mol^{-1} in B1 and by 0.7 kcal mol^{-1} in B2. This phenomenon is further discussed below.

A number of residues, such as K28, Y33, N35, and T55, have ΔG_{op} approximately equal to ΔG_u in B2 but not in B1, with $\Delta\Delta G_{op} \approx 0$ kcal mol^{-1} (Figures 4 and 5). For these residues, the difference in exchange rates between B2 and B1 is small and does not reflect the global stability difference (Table 1). Therefore, these residues do not exchange through global unfolding but rather through a high-energy local unfolding mechanism. Here, we assume that a 1 kcal mol^{-1} stabilization of the protein would not convert a global unfolder in B2 to a local unfolder in the more stable B1 domain. Therefore, these residues are designated as local unfolders in both B1 and B2. In an earlier paper (Orban et al., 1994), we suggested that all residues in B2 with ΔG_{op} approximately equal to ΔG_u were consistent with global unfolding. However, the present study shows that it is not possible to distinguish global unfolding from high-energy local unfolding using exchange rates in B2 alone. Comparison of exchange rates in B1 and B2 enables differentiation between local and global unfolding for most residues. This is because slow exchange ΔG_{op} values are not as clustered in B1 as in B2 due to the additional 1 kcal mol^{-1} stabilization of global unfolders (Figure 4). For residues with ΔG_{op} values that are less than ΔG_u, exchange takes place through varying degrees of smaller amplitude local fluctuations in the structure.

The temperature dependence of ΔG_{op} for H-bonded NHs in B1 and B2 is shown in Figure 7. Exchange rates were measured from 25 to 65 °C for B1 and from 25 to 60 °C for B2. At higher temperatures, exchange rates could not be measured accurately and the EX_2 mechanism, where $k_f \gg k_u$ and $k_f \gg k_c$, is no longer valid (Roder et al., 1985; Roder, 1989). For global unfolders in B1, ΔG_{op} approximates ΔG_u over most of the temperature range sampled although ΔG_{op} is ca. 1 kcal mol^{-1} greater than ΔG_u for a number of residues in the $\beta3-\beta4$ region at 25 °C. For faster exchanging NHs, where ΔG_{op} is less than ΔG_u, exchange occurs through smaller-amplitude local unfolding pathways at 25 °C. As the temperature is increased, the ΔG_{op} for these NHs converges on ΔG_u, indicating that global unfolding becomes the dominant exchange mechanism at higher temperatures. Similar observations have been made for BPTI (Kim & Woodward, 1993) and cytochrome *c* (Bai et al., 1994). As mentioned above, it is more difficult to distinguish global from local unfolders in B2 than B1. This is also evident from analysis of ΔG_{op} versus temperature. For example, the temperature dependence of ΔG_{op} for T55 shows that it is a high-energy local unfolder in B1 (Figure 7c) but cannot be differentiated from global unfolders in B2 (Figure 7f). The results presented here show that the ΔG_{op} values obtained from H−D exchange measurements and calorimetric ΔG_u provide highly complementary information on the ΔG versus temperature stability profiles of B1 and B2. The H−D exchange measurements have the advantage of providing ΔG values for individual NHs.

Three residues, K31, A34, and D46, cannot be classified definitively as either global or local unfolders since ΔG_{op} approximates ΔG_u in B1 and B2 but $\Delta\Delta G_{op} \approx 0.3$ kcal mol^{-1} (Figures 4 and 5). For K31 and D46, ΔG_{op} is 0.6−0.8 kcal mol^{-1} greater than ΔG_u in B2 but is approximately equal in B1 at 25 °C. The temperature dependent behavior of ΔG_{op} for K31 appears to be consistent with large-amplitude global unfolding in B1 and B2 (Figure 7b,e). Similar behavior is observed for D46 although the ΔG_{op} is 1 kcal mol^{-1} lower than the averaged value for T44, T51, F52, T53, and V54 at 25 °C. For A34, ΔG_{op} is 0.3 kcal mol^{-1} less than the extrapolated ΔG_u in B1 at 25 °C and converges with ΔG_u at 40 °C (Figure 7b). This suggests that A34 may exchange through a high-energy local rather than through a global unfolding mechanism.

For residues Y3 and T18, ΔG_{op} is significantly less than ΔG_u in the B2 domain, and therefore exchange occurs through a local unfolding mechanism (Figures 4 and 7d). However, $\Delta\Delta G_{op}$ is greater than 2 kcal mol^{-1} for both of these residues (Figure 5), indicating relatively large changes in local stability between B2 and B1. In the more stable B1 domain, ΔG_{op} approximates ΔG_u for Y3 and T18 (Figures 4 and 7a), indicating that these residues may now exchange through a global unfolding mechanism. Thus, the B1 domain appears to have a slightly larger core of residues which exchange by global unfolding than B2.

Local Stability Differences between B1 and B2. The largest local stability differences occur at residues Y3 and T18, which exchange 40-fold and 100-fold slower in B1, respectively (Table 1, Figure 3). These residues form a H-bond donor−acceptor pair at one end of the $\beta1-\beta2$ hairpin (Figure 6). Local stability differences are also observed at neighboring residues such as T2, A20, and T16, although these $\Delta\Delta G_{op}$ values are smaller than for Y3 and T18 (Figure 5). Two of the six variant residues between B1 and B2 (Figure 6) occur in this region at positions 19 and 29. The E19K substitution (B1 to B2) has no effect on the intrinsic exchange rate of T18 and an approximately 2-fold enhancement of the intrinsic exchange rate of A20. The nearest-neighbor side-chain effects of residue 19 do not account for the large observed differences in exchange rates between B1 and B2 for Y3, T18, and A20 (Table 1). Therefore, other effects due to tertiary structure must be responsible for the large rate differences. One possible reason for increased stabilization in this region of the $\beta1-\beta2$ hairpin may be due to the A29V substitution in going from B2 to B1. This may lead to improved hydrophobic contacts between methyl groups from V29 and T18 (Figure 6), which would stabilize the β2-strand and slow exchange at T18, its H-bond partner Y3, and also neighboring residues. Indeed, preliminary investigations in our laboratory show that mutation of alanine to valine at position 29 stabilizes B2 by 4 °C, which is half of the stability difference between B1 and B2. This stabilizing effect may be subtle from a structural viewpoint. The distance beween the nearest γ-methyl carbon of V29 and the methyl carbon of T18 is ~4.6 Å in B1 (Gallagher et al., 1994). In B2, the distance from the β-methyl carbon of A29 to the methyl carbon of T18 is also ~4.6 Å (Achari et al., 1992). There is some adjustment in the structure of B1 to accommodate the larger valine residue at position 29 in the helix. There are no direct Van der Waals contacts

between V29 and Y3 and only weak V29−A20 and V29−T16 interactions.

Stabilizing effects on non-H-bonded NHs in this region of the $\beta1-\beta2$ hairpin, such as residues 17, 19, and 21, are small with $\Delta\Delta G_{op} \leq 0.4$ kcal mol^{-1} (Figure 5). The exception is T2, for which $\Delta\Delta G_{op} \geq 0.6$ kcal mol^{-1}. Exchange is slower in B1 than B2 even though the NH of T2 is not H-bonded. This may be partly due to more local rigidity in B1 than B2 [cf. Kim et al. (1993)]. Additional stabilization in B1 may come from a favorable electrostatic interaction between the γ-carboxylate group of E19 and the N-terminal ammonium group of M1 (Figure 6) although this effect is expected to be attenuated at pD 3.1 where non-H-bonded NH exchange rates were measured.

Local stability differences are also evident at the other end of the $\beta1-\beta2$ hairpin, near the $\beta1-\beta2$ turn. The largest stability difference for a fast exchange NH is observed for L12, where $\Delta\Delta G_{op} \geq 0.9$ kcal mol^{-1} (Figure 5). In B1, L12 is in close contact with L7 (Figure 6), whereas in B2, position 7 is an isoleucine. The exchange rate measurements suggest that the Van der Waals interactions between L7 and L12 are more favorable than when an isoleucine occupies position 7. Again, the differences in structure in this region appear to be quite small. The closest contacts between residues 7 and 12 are similar (±0.1 Å) in B1 and B2, although L12 is disordered and exists in two discrete conformers in B2 (Achari et al., 1992) but not in B1 (Gallagher et al., 1994). Only lower limit values of $\Delta\Delta G_{op}$ could be obtained for K10 and T11 due to their faster-than-expected exchange behavior (see below). Thus, while there is no correlation between fast exchange rates and global stability, there appears to be a correlation with local stability in protein G.

The B1 domain is approximately 1 kcal mol^{-1} more stable than B2. The reasons for this stability difference do not seem to be readily apparent from inspection of the X-ray structures although improved hydrophobic contacts are implicated from an A29V stability mutant of B2. However, differences in local and global stability between the two domains are manifested as readily measurable changes in NH exchange rates for individual residues. Therefore, NH exchange rates provide a very sensitive measure of stability differences which are, at least in part, due to hydrophobic packing effects. Knowledge of these local stability differences in the $\beta1-\beta2$ region provides potential approaches for designing new stability mutants in protein G.

Amide Protons with $k_{ex} > k_c$. Most non-H-bonded NHs have exchange rates which are <15 times slower than their intrinsic rates [Table 1; cf. Tuchsen and Woodward (1985)]. In marked contrast, exchange rates for K10, T11, and L12 in the $\beta1-\beta2$ turn are significantly faster than their intrinsic rates (five to ≥24 times), leading to negative ΔG_{op} values for these residues (Table 1; Figure 4). The X-ray structure of B1 shows that the $\beta1-\beta2$ turn is capped by stabilizing H-bonds from (1) the ϵ-ammonium group of K13 to the carbonyl groups of G9 and K10, and from (2) the γ-carboxylate group of E56 to the NH of K10 (Figure 6; Gallagher et al., 1994). Similar features are observed for the $\beta1-\beta2$ turn in the B2 X-ray structure (Achari et al., 1992). Residues T11 and L12 are not H-bonded in the X-ray structures. In the solution structure for B1 (Gronenborn et al., 1991), the carbonyl group of G9 is H-bonded to the NH of L12 rather than the ϵ-ammonium group of K13. The exchange rate data

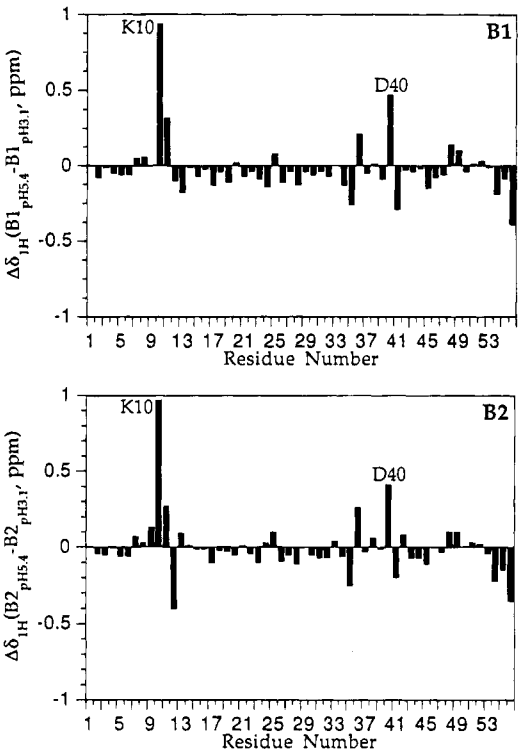

FIGURE 8: ^{1}H chemical shift difference (pH 5.4 − pH 3.1) plots for main-chain NHs in B1 and B2 at 25 °C.

presented here are not consistent with L12 being H-bonded in B1 or B2, however.

At the solution conditions used for measurement of fast exchange NHs (pD 3.1), the γ-carboxylate of E56 is expected to be protonated at least partially. An approximately 1.0 ppm upfield shift for the NH of K10 is observed in going from pH 5.4 to pH 3.1 (Figure 8). This is consistent with titration of the E56 side chain and a decrease in H-bonding to K10. In addition, a smaller upfield shift of 0.4−0.5 ppm is observed for the NH of D40 which is also within H-bonding distance of the γ-carboxylate of E56 but with poorer geometry (Gallagher et al., 1994). Under these conditions, the presence of the positively charged side chain of K13 near carbonyl groups in the $\beta1-\beta2$ turn is likely to withdraw electron density from the peptide NHs, making the NHs more acidic than they would be in an unstructured peptide. In addition, the three proximal NHs of K10, T11, and L12 are pointing in the same direction and may generate a positive local electrostatic field. This would increase local hydroxide ion concentration which may also contribute to acceleration of NH exchange rates beyond their intrinsic rates. Under the present solution conditions (pD 3.1), hydroxide ion is still a significant contributor to NH exchange (Wagner, 1983; Englander & Kallenbach, 1984).

An analogous rate enhancement is observed for the NH of V21 (Table 1; Figure 4). The adjacent carbonyl group of A20 is within H-bonding distance of the positively charged N-terminal ammonium group of M1 (Figure 6) and a similar mechanism for rate enhancement probably exists. Therefore, the accelerated rates for K10, T11, L12, and V21 indicate that they exchange through a conformation approximated by the folded state.

Comparison of NH Exchange Rates with NMR and X-ray Data. Analysis of exchange rate differences between the N- and C-terminal halves of the helix suggests that they may

be different structurally and/or dynamically (Table 1; Figure 4). This is consistent with results from other solution studies. For example, in the solution structure of B1, residues 22–32 form an α-helix and residues 33–37 form a 3_{10}-helix (Gronenborn et al., 1991). Furthermore, order parameters from ^{15}N-relaxation measurements on B1 indicate more mobility at the C-terminal end of the helix (Barchi et al., 1994). In contrast, no helical discontinuity is observed in the X-ray structures of B1 and B2, and both domains have α-helices from residue 23 to residue 38 (Achari et al., 1992; Gallagher et al., 1994). Crystallographic temperature factors for main-chain atoms are approximately the same for H-bonded residues in both halves of the helix.

The exchange rates of H-bonded NHs indicate that the β2-strand is the least stable, and therefore most mobile, of the β-sheet. Order parameters in B1 also indicate more mobility in the β2-strand (Barchi et al., 1994). However, the differences in order parameters between the β2-strand and the rest of the β-sheet are small compared with the relatively large differences in NH exchange rates (Table 1; Figure 4). Thus, the NH exchange data may provide a qualitative but more sensitive measure of main-chain mobility than order parameters. Similar observations have been made in comparing NH exchange and ^{15}N-relaxation data in reduced and oxidized *Escherichia coli* thioredoxin (Jeng & Dyson, 1995). The main-chain temperature factors are only slightly higher in the β2-strand than the rest of the β-sheet for both B1 and B2 X-ray structures (Achari et al., 1992; Gallagher et al., 1994). This is probably due to the fact that intermolecular H-bonding exists between the β2-strand of one protein G molecule and the β3-strand of another in B1 and B2 crystals. In this case, crystal contacts perturb main-chain dynamics and complicate comparison of temperature factors with NH exchange data.

Comparison of ΔG_{op} with ΔG_u. Implications for the Unfolded State and Folding. In the calculation of ΔG_{op}, the NH exchange rate in the unfolded state is equated with the intrinsic exchange rate, k_c, which is determined for an unstructured peptide. However, if the unfolded state possesses residual structure, k_c will be an overestimate of the exchange rate in the unfolded state. From eq 4, this would lead to an overestimate of ΔG_{op} for residues involved in the residual structure. In B1 and B2 at 25 °C, ΔG_{op} values for some residues in the β3–β4 hairpin region are up to 1 kcal mol^{-1} higher than the extrapolated ΔG_u (Figure 4). Similarly, ΔG_{op} is greater than ΔG_u for some residues in the N-terminal half of the helix in B1 and B2 although the differences are smaller. These results suggest that some residual structure may exist in the β3–β4 region in the "unfolded state" and perhaps also in the N-terminal half of the helix. The temperature dependence of ΔG_{op} for residues T44, T51, F52, T53, and V54 in the β3–β4 hairpin of B1 shows that, while the average ΔG_{op} is ~1 kcal mol^{-1} higher than ΔG_u at 25 °C, it converges on the extrapolated ΔG_u as the temperature is increased (Figure 7c). Analogous temperature dependent behavior is observed in B2 (Figure 7f). The convergence of elevated ΔG_{op} with ΔG_u is consistent with a decrease in β3–β4 hairpin residual structure in the unfolded state as the temperature is increased. This is one possible interpretation of the elevated ΔG_{op} values in the β3–β4 region.

A potential limitation of this analysis is the accuracy of extrapolation of calorimetric data near the thermal transition to lower temperatures. Nevertheless, the exchange rates presented here indicate that the β3–β4 hairpin region is more stable than the β1–β2 hairpin region and may therefore be more populated in transient folding intermediates which are in dynamic equilibrium with the unfolded state. This is consistent with kinetic pulse-labeling data on B1 which show that slow exchange residues in the β3–β4 region have slightly higher protection factors than other slow exchange residues in the β-sheet (Kuszewski et al., 1994). Interestingly, the highest protection factors in the helix were observed in the N-terminal end. Furthermore, recent studies show that the peptide corresponding to residues 41–56 in the β3–β4 hairpin of B1 possesses some native-like structure as determined by CD and NMR measurements (Blanco et al., 1994). In contrast, peptides corresponding to the helix and β1–β2 hairpin were found to be predominantly unstructured in water (Blanco & Serrano, 1995).

Analysis of the present data suggests that some residual structure may exist in the unfolded state of protein G, although further experiments are needed to establish this conclusively. Comparison of ΔG_{op} with the extrapolated ΔG_u as a function of temperature may provide information about the unfolded state under native, nondenaturing conditions.

SUPPORTING INFORMATION AVAILABLE

Table of ^{1}H and ^{15}N chemical shifts for main-chain NHs in B1 and B2 at pH 5.4 and at pH 3.1, 25 °C (3 pages). Ordering information is given on any current masthead page.

REFERENCES

Achari, A., Hale, S. P., Howard, A. J., Clore, G. M., Gronenborn, A. M., Hardman, K. D., & Whitlow, M. (1992) *Biochemistry 31*, 10449–10457.

Akerstrom, B., & Bjorck, L. (1986) *J. Biol. Chem. 261*, 10240–10247.

Alexander, P., Fahnestock, S., Lee, T., Orban, J., & Bryan, P. (1992a) *Biochemistry 31*, 3597–3603.

Alexander, P., Orban, J., & Bryan, P. (1992b) *Biochemistry 31*, 7243–7248.

Bai, Y., Milne, J. S., Mayne, L., & Englander, S. W. (1993) *Proteins 17*, 75–86.

Bai, Y., Milne, J. S., Mayne, L., & Englander, S. W. (1994) *Proteins 20*, 4–14.

Barchi, J. J., Jr., Grasberger, B., Gronenborn, A. M., & Clore, G. M. (1994) *Protein Sci. 3*, 15–21.

Bax, A., Griffey, R. H., & Hawkins, B. L. (1983) *J. Magn. Reson. 55*, 301–315.

Bax, A., Ikura, M., Kay, L. E., Torchia, D. A., & Tschudin, R. (1990) *J. Magn. Reson. 86*, 304–318.

Becktel, W. J., & Schellman, J. A. (1987) *Biopolymers 26*, 1859–1877.

Blanco, F. J., & Serrano, L. (1995) *Eur. J. Biochem. 230*, 634–649.

Blanco, F. J., Rivas, G., & Serrano, L. (1994) *Nature Struct. Biol. 1*, 584–590.

Bodenhausen, G., & Ruben, D. J. (1980) *Chem. Phys. Lett. 69*, 185–189.

Brandts, J. F. (1964) *J. Am. Chem. Soc. 86*, 4291–4301.

Englander, S. W., & Kallenbach, N. R. (1984) *Q. Rev. Biophys. 16*, 521–655.

Englander, S. W., & Mayne, L. (1992) *Annu. Rev. Biophys. Biomol. Struct. 21*, 243–265.

Fahnestock, S. R., Alexander, P., Nagle, J., & Filpula, D. (1986) *J. Bacteriol. 167*, 870–880.

Gallagher, T., Alexander, P., Bryan, P., & Gilliland, G. L. (1994) *Biochemistry 33*, 4721–4729.

Gouda, H., Torigoe, H., Saito, A., Sato, M., Arata, Y., & Shimada, I. (1992) *Biochemistry 31*, 9665−9672.
Gronenborn, A. M., & Clore, G. M., (1993) *J. Mol. Biol. 233*, 331−335.
Gronenborn, A. M., Bax, A., Wingfield, P. T., & Clore, G. M. (1989) *FEBS Lett. 243*, 93−98.
Gronenborn, A. M., Filpula, D. R., Essig, N. Z., Achari, A., Whitlow, M., Wingfield, P. T., & Clore, G. M. (1991) *Science 253*, 657−661.
Hvidt, A., & Nielsen, S. O. (1966) *Adv. Protein Chem. 21*, 287−386.
Jeng, M.-F., & Dyson, H. J. (1995) *Biochemistry 34*, 611−619.
Kim, K.-S., & Woodward, C. K. (1993) *Biochemistry 32*, 9609−9613.
Kim, K.-S., Fuchs, J. A., & Woodward, C. K. (1993) *Biochemistry 32*, 9600−9608.
Kraulis, P. J. (1991) *J. Appl. Crystallogr. 24*, 946−950.
Kuszewski, J., Clore, G. M., & Gronenborn, A. M. (1994) *Protein Sci. 3*, 1945−1952.
Lian, L.-Y., Yang, J. C., Derrick, J. P., Sutcliffe, M. J., Roberts, G. C. K., Murphy, J. P., Goward, C. R., & Atkinson, T. (1991) *Biochemistry 30*, 5335−5340.
Lian, L.-Y., Derrick, J. P., Sutcliffe, M. J., Yang, J. C., & Roberts, G. C. K. (1992) *J. Mol. Biol. 228*, 1219−1234.
Marion, D., & Wuthrich, K. (1983) *Biochem. Biophys. Res. Commun. 113*, 967−974.
Marion, D., Ikura, M., Tschudin, R., & Bax, A. (1989) *J. Magn. Reson. 85*, 393−399.
Myhre, E. B., & Kronvall, G. (1977) *Infect. Immun. 17*, 475−482.
Norwood, T. J., Boyd, J., Heritage, J. E., Soffe, N., & Campbell, I. D. (1990) *J. Magn. Reson. 87*, 488−501.
Orban, J., Alexander, P., & Bryan, P. (1992) *Biochemistry 31*, 3604−3611.
Orban, J., Alexander, P., & Bryan, P. (1994) *Biochemistry 33*, 5702−5710.
Pace, C. N., & Tanford, C. (1968) *Biochemistry 7*, 198−208.
Privalov, P. L. (1979) *Adv. Protein Chem. 33*, 167−241.
Privalov, P. L., & Khechinashvili, N. N. (1974) *J. Mol. Biol. 86*, 665−684.
Reis, K. J., Ayoub, E. M., & Boyle, M. D. P. (1984) *J. Immunol. 132*, 3098−3102.
Roder, H. (1989) *Methods Enzymol. 176*, 446−473.
Roder, H., Wagner, G., & Wuthrich, K. (1985) *Biochemistry 24*, 7396−7407.
Shaka, A. J., Barker, P. B., & Freeman, R. (1985) *J. Magn. Reson. 64*, 547−552.
Stone, G. S., Sjobring, U., Bjorck, L., Sjoquist, J., Barber, C. V., & Nardella, F. A. (1989) *J. Immunol. 143*, 565−573.
Tuchsen, E., & Woodward, C. (1985) *J. Mol. Biol. 185*, 405−419.
Wagner, G. (1983) *Q. Rev. Biophys. 16*, 1−57.
Woodward, C., Simon, I., & Tuchsen, E. (1982) *Mol. Cell. Biochem. 48*, 135−160.
Wright, C., Willan, K., Sjodahl, J., Burton, D. R., & Dwek, R. (1977) *J. Biochem. 167*, 661−668.

BI951273N